Check for updates

Fabrication and photochromic properties of Forcespinning® fibers based on spiropyran-doped poly(methyl methacrylate)

Hoan Ngoc Doan,[ae] Hayato Tsuchida,[b] Takato Iwata,[c] Kenji Kinashi, [ID] *[d] Wataru Sakai,[d] Naoto Tsutsumi[d] and Dai Phu Huynh[e]

Spiropyran-functionalized poly(methyl methacrylate) (PMMA) Forcespinning® fibers were fabricated using a fiber making machine of our own design, employing 1′,3′,3′-trimethyl-6-nitrospiro[1(2H)-benzopyran-2,2′-indoline] (6-nitro BIPS) as the spiropyran. The effects of the polymer solution concentration (and hence the viscosity), the spinneret rotational rate, and the internal needle diameter on the formation and morphology of the fibers were examined, using scanning electron microscopy. A rotational speed of 3000 rpm and an internal nozzle diameter of 0.35 mm (23 G) in conjunction with a polymer concentration of 15 wt% produced 6-nitro BIPS/PMMA Forcespinning fibers having a smooth morphology with no beads. The photochromic properties of the resultant fibers were characterized by reflectance spectroscopy using the Kubelka–Munk function, fluorescence excitation emission matrix (EEM) analysis, and Raman spectroscopy. The thermal decoloration dynamics of the 6-nitro BIPS in the PMMA fibers were in good agreement with the properties observed in films. These results suggest that 6-nitro BIPS and other spiropyran dyes have significant potential as probes to assess the structures of micro/nanofibers.

Introduction

Micro/nanofibers have many unique characteristics, such as high surface-to-mass (or volume) ratios, and the ability to form highly porous fibrous membranes. Nanofibers can be produced by melt blowing, flash-spinning, bicomponent spinning, and Forcespinning (or centrifugal spinning).[1] Electrospinning can also be used to fabricate micro/nanofibers, and electrospun fibers have been used for applications such as filters, scaffolds, enzyme carriers, and sensors.[2–5] However, electrospinning processes suffer from many drawbacks, including low productivity (with maximum rates of 300 mg h^{-1}),[6] the requirement to use an additional solvent extraction process, and environmental concerns related to the use of toxic solvents. To address the disadvantages associated with electrospinning, a novel spinning method termed Forcespinning™ (hereinafter "forcespinning") was developed by Lozano *et al.*[7,8] In this process, the

electric field normally employed in electrospinning is replaced by centrifugal force. The limitations of the electrospinning process, such as the requirement to apply a very high electric field, low productivity, and high production costs, are eliminated in forcespinning. Forcespinning also broadens the selection of materials that can be employed, as both conductive and non-conductive materials can be spun into micro/nanofibers. Another noteworthy feature of forcespinning fibers is that these fibers are readily functionalized using functional polymers or by adding functional dyes into the initial polymer solution. This unique feature in anticipated to lead to numerous applications for forcespun micro/nanofibers as smart textiles.[9]

Photochromic dyes, such as spiropyrans (**SP**s), are both functional and dispersible, and the chemical structure of the **SP**s is similar to that of traditional dispersible dyes that are used for textiles. One unique property of photochromic dyes—reversible photoisomerization—has attracted considerable interest with regard to applications in photochromic windows and eye-protection, rewritable optical data storage,[10] drug delivery system,[11] mechanophores,[12] and X-ray radiation detection.[13,14] **SP** dyes consist of two heterocyclic moieties linked together by an sp^3 hydridized spirocarbon atom. Irradiation by UV light and/or a temperature increase can cleave the relatively weak spirocarbon–oxygen (C–O) bond. This is followed by conformational rearrangement to a ring-opened colored isomer: the so-called photomerocyanine form (PMC-form) with

[a]Internship Student, Kyoto Institute of Technology, Matsugasaki, Sakyo, Kyoto 606-8585, Japan
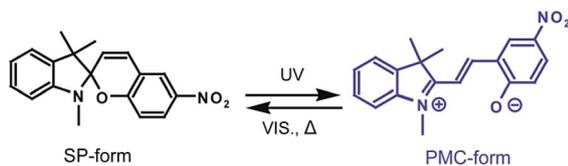*[b]Master's Program of Innovative Materials, Graduate School of Science and Technology, Kyoto Institute of Technology, Matsugasaki, Sakyo, Kyoto 606-8585, Japan*
[c]School of Science and Technology, Kyoto Institute of Technology, Matsugasaki, Sakyo, Kyoto 606-8585, Japan
[d]Faculty of Materials Science and Engineering, Kyoto Institute of Technology, Matsugasaki, Sakyo, Kyoto 606-8585, Japan. E-mail: kinashi@kit.ac.jp
[e]Faculty of Materials Technology, University of Technology, Vietnam National University, HoChiMinh City, Vietnam

Scheme 1 Photoisomerization of a spiropyran.

Fig. 1 (a) Schematic diagram of the forcespinning system used in this work and a side view of the polymer solution jet. Photographs of the apparatus (b) before and (c) after forcespinning.

a high molar absorption coefficient, as shown in Scheme 1. The PMC-form reverts to the closed-ring isomer (the **SP**-form) through a thermally induced ring closure reaction, accompanied by fading of the colored isomer on a timescale of seconds to minutes at room temperature. The PMC-form can function as a molecular probe since its decoloration dynamics or fluorescent properties can be tracked to assess internal polymer properties.[15]

In the present study, **SP**-functionalized poly(methyl methacrylate) (PMMA) forcespinning fibers were fabricated using an apparatus of our own design. The aim of this research was to investigate the formation of these fibers and the effects of various parameters, including the concentration of the polymer solution (as reflected in the viscosity), the spinneret rotational rate, and the internal needle diameter, on the fiber morphology and photochromic properties of the fibers.

Experimental

Materials

All chemicals were commercially available and used without further purification. The photochromic **SP** dye 1′,3′,3′-trimethyl-6-nitrospiro[1(2H)-benzopyran-2,2′-indoline] (or 1,3,3-trimethyl-lindolino-6′-nitrobenzopyrylospiran) (6-nitro BIPS), acetone and chloroform were purchased from the Tokyo Kasei Co. PMMA was purchased from the Nacalai Tesque Co.

Sample preparation for forcespinning

A series of viscous polymer solutions was obtained by dissolving both 6-nitro BIPS and PMMA in chloroform/acetone (3 : 1 w/w) with stirring at room temperature for 30 min. The mixed solvent was used to increase an evaporating efficiency. The PMMA in these solutions was varied from 1 to 17 wt%. The concentration of the 6-nitro BIPS was fixed at 0.03 wt% regardless of the PMMA concentration. The dye concentration 0.03 wt% is an appropriate concentration from the point of view of photochromic reaction in fiber.[13] The viscous polymer solutions were further mixed using a planetary centrifugal mixer (ARE-310, Thinky Co.) at 2000 to 4000 rpm, employing approximately 1 cm diameter polystyrene balls, for 30 min. The viscosity of each solution was measured with a vibronic viscometer (SV-1A, A&D Co.) at room temperature (25 °C).

PMMA fibers containing 6-nitro BIPS at 0.03 wt% were prepared using a forcespinning apparatus of our own design. This system consisted of a 60 mm needle-base spinneret equipped with blunt needles, rotated with an AC motor (EUROST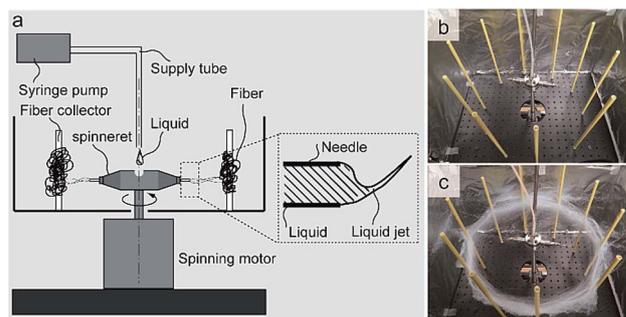AR 20 high-speed digital, IKA Co.). The loading rate of the viscous polymer solution was controlled by a syringe pump (KDS-100, KD Scientific Co.) at 50 μL h^{-1}. The distance between the tip of each needle and the collectors was 290 mm. A schematic illustration of the device and photographic images before and after spinning are shown in Fig. 1.

Measurements

The weight-average molecular weight (M_w) and number-average molecular weight (M_n) of the PMMA were determined by gel permeation chromatography (GPC) using a Shodex GPC System-21 (Showa Denko Co.) equipped with G5000–G3000 columns and with tetrahydrofuran (THF) as the eluent. The system was calibrated using polystyrene standards. The M_w of the PMMA was 100 664 g mol^{-1} and its polydispersion index, $M_\mathrm{w}/M_\mathrm{n}$, was 1.8. The morphology of the resulting fibers was characterized using scanning electron microscopy (SEM) (S-3000N, Hitachi Co.). The diameters and size distributions of the fibers ($n = 100$) were determined from the SEM images using image processing software (ImageJ and Minitab). UV-vis reflectance spectra were recorded with a spectrophotometer (HSU-100H, Asahi spectra Co.).

Color strengths (corresponding to K/S peaks) of the fibers were calculated using the Kubelka–Munk equation:

$$K/S = (1 - R)^2/2R,$$

where R is the observed reflectance, K is the absorption coefficient and S is the light scattering coefficient. An excitation wavelength of 360 nm (4.1 mW cm^{-2}), obtained by passing the light from a Xe arc lamp (MAX-303, Asahi Spectra Co.) through a band-pass filter (MX0360, Asahi Spectra), was employed to generate the PMC-form of the dye.

Fluorescence excitation emission matrix (EEM) was analysed using a photoluminescence spectrophotometer (RF-6000, Shimadzu Co.). Fluorescence quantum yield (Φ_F) was measured by a photoluminescence spectrophotometer (RF-6000, Shimadzu Co.) with a 100 mm diameter Spectralon integrated sphere unit. The measurement was carried out after 360 nm light irradiation for 1 min. All of the Raman measurement were performed at room temperature using a laser Raman microscope (Nanophoton, Raman-11). In this study, we chose a 785 nm excitation laser with which the 6-nitro BIPS is not resonant.

Results and discussion

The forcespinning system consisted of a spinneret, fiber collectors, syringe pump, supply tube and spinning motor. The viscous polymer solution was fed continuously into the spinneret and the polymer solution was centrifugally forced through the needles to discharge beads, beaded fibers, or fibers. The morphologies of the resulting fibers varied greatly with the polymer solution employed, especially with the viscosity of the solution. The effect of the solution concentration on the diameters of the 6-nitro BIPS/PMMA forcespinning fibers was assessed using SEM images, as shown in Fig. 2, using an internal nozzle diameter of 0.34 mm (23 G) at a rotational rate of 3000 rpm. It was found that 6-nitro BIPS/PMMA forcespinning fibers or beaded fibers could be produced using concentrations in the range from 9 to 17 wt% (equivalent to relatively high viscosities of 15.9 to 104 mPa s). At lower viscosities (less than 2 wt%; equivalent to 0.96 mPa s), the polymer solutions produced a film on the aluminum foil around the collectors, indicating that continuous fibers were not produced. It was also possible to generate polymer beads at moderate concentrations ranging from 3 to 8 wt% (1.71 to 10.05 mPa s). According to the SEM images, the minimum concentration necessary to obtain uniform 6-nitro BIPS/PMMA forcespinning fibers is 15 wt%. Above this value, the degree of polymer entanglement is suitable for forcespinning, and uniform fibers with an equivalent diameter of 8.56 μm or greater are produced. At concentrations above 17 wt%, the centrifugal force generated by a spinneret rotation of 3000 rpm is insufficient to overcome the surface tension, so jets and fiber elongation are not obtained and droplets are not formed. Based on these data, entanglement concentration is evidently an important factor in the force-spinning process.

The concept of a characteristic polymer solution concentration, the critical chain overlap concentration, C^*, is introduced herein to facilitate the data interpretation. Physically, C^* is the point at which the concentration inside a single macromolecular chain equals the solution concentration. This value is approximately equal to $1/[\eta]$, where $[\eta]$ is the intrinsic viscosity of the polymer solution. Using C^*, it is easier to recognize the concentration at which the transition between dilute and semi-dilute regimes occurs. The dimensionless product of the intrinsic viscosity $[\eta]$ and the concentration of the polymer solution C, $[\eta]$ C, is referred to as the Berry number, and a value above unity indicates a solution having chain entanglements.[16] In this study, $[\eta]$ was calculated using the Mark–Houwink–Sakurada equation: $[\eta] = KMa$.[17] Here, the values of Mark–Houwink constants K and a are dependent on the nature of the polymer, the solvent and the temperature, and M is the molecular weight. The K and a values for PMMA at 30 °C in THF have been reported by the American Polymer Standards Corp. as 0.0128 g cm^{-3} and 0.690, respectively. Based on these parameters, the intrinsic viscosity of PMMA is estimated to be 36.24 cm^3 g^{-1}.

The critical chain overlap concentration, C^*, can then be calculated as approximately $1/[\eta]$. Converting this C^* gives a concentration of 3.0 wt% (taking the specific gravity of THF as 0.89 g cm^{-3}). This result is consistent with data reported by Gupta *et al.*, who determined the critical chain overlap concentrations of PMMA samples with various molecular weights in dimethyl formamide using the Mark–Houwink–Sakurada equation.[18] The viscosity, η, of a polymer solution measured using a vibronic viscometer at a low frequency of 30 Hz can be regarded as the zero-shear viscosity, η_0, and experimental η values are plotted as a function of the concentration divided by C^* in Fig. 3. The resulting plots of the viscosity values against C/C^* can be separated into different solution regimes: dilute ($C/C^* < 0.9$, 1–2 wt%), semi-dilute unentangled ($0.9 < C/C^* \leq 2.7$, 3–8 wt%) and semi-dilute entangled ($C/C^* > 2.7$, 9–17 wt%). These results are in good agreement with data reported for PMMA in DMF obtained using dynamic light scattering.[18] The concentration of the polymer solution in the dilute regime ($C/C^* < 0.9$) results in insufficient chain overlap, leading to the formation of polymer films (as determined by SEM images but not shown in Fig. 2). This outcome indicates a lack of solvent evaporation during the forcespinning process. Beyond the dilute regime, two distinct
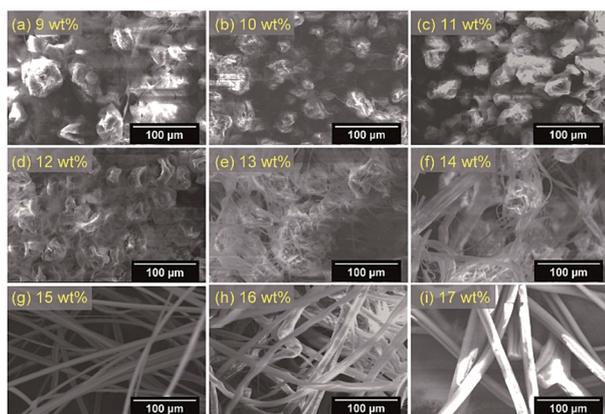

Fig. 2 SEM images of 6-nitro BIPS/PMMA forcespinning fibers prepared with different polymer solution concentrations: (a) 9, (b) 10, (c) 11, (d) 12, (e) 13, (f) 14, (g) 15, (h) 16, and (i) 17 wt%. Forcespinning conditions: 290 mm needle to collectors distance, 0.34 mm 23 G needle nozzle, spinneret rotational rate of 3000 rpm.
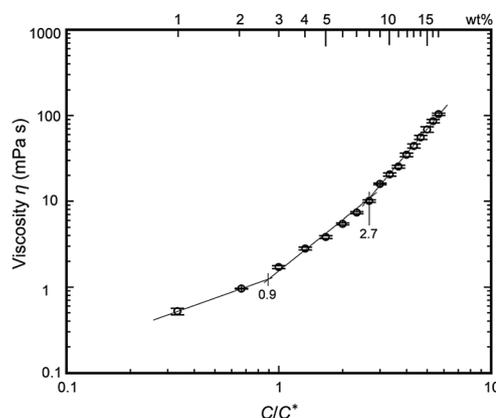

Fig. 3 Correlation of viscosity, η, with C/C^* for the various polymer solutions.

regimes appear, as indicated by the change in the slope of the data. As the concentration is increased to the semi-dilute unentangled regime at $0.9 < C/C^* \leq 2.7$, polymer droplets are observed. This result suggests that the semi-dilute unentangled solutions lead to the formation of only droplets, due to insufficient chain entanglements. Based on the SEM images obtained in conjunction with the semi-dilute entangled solutions at $C/C^* > 2.7$, solutions with concentrations in the range of 9–14 wt% produce fibers containing some beads, while smooth fibers result from concentrations in the range of 15–17 wt%. Furthermore, the crossover between the semi-dilute unentangled and entangled regimes occurs at $C/C^* = 2.7$ (9 wt%), which corresponds to the critical chain entanglement concentration, C_e. Thus, in the case of a PMMA solution containing 6-nitro BIPS, the formation of fibers requires $C/C^* > 2.7$ (9 wt%), at which point the chain entanglement is sufficient to produce uniform and continuous bead-free fibers. In addition, the SEM image in Fig. 2 shows that a concentration at which C/C^* is approximately 5.0 (15 wt%) is required for fibers having a smooth morphology with no beads. The average diameter of the 6-nitro BIPS/PMMA forcespinning fibers generated in the semi-dilute entangle regime at $5.0 < C/C^* < 5.7$ and 23 G (3000 rpm) was subsequently measured from SEM images.

Fig. 4 shows the distributions of fiber diameters resulting from polymer solutions in the semi-dilute entangled regime at $5.0 < C/C^* < 5.7$ (15–17 wt%), and the relationship between the average fiber diameter and polymer concentration. The fiber diameters were found to be 8.6 ± 2.8 μm, 10.0 ± 6.0 μm, and 26.1 ± 6.7 μm, respectively, at the three concentrations. These results show that the fiber diameter increases with increasing concentration of the polymer solution in the semi-dilute entangled regime. In particular, the lowest polymer concentration (15 wt%) results in weak linkages that allow the rapid break-up of chain entanglements within the jet, forming fibers with narrow and uniform diameters.

The effect of the spinneret rotational rate on the fiber diameter distributions when using a polymer concentration of $C/C^* = 5$ (15 wt%) was assessed with an internal nozzle diameter of 0.34 mm (23 G). The rotational rates ranged from 1000 to 6000 rpm. At 1000 rpm, the centrifugal force was low, so the fibers were pulled back onto the rotating shaft and could not be collected. Rotational rates of 5000 and 6000 rpm resulted in a high centrifugal force exerted on the polymer solution, such that the jet was scattered and only beads were produced. Fig. 5 presents SEM images and fiber diameter distributions corresponding to various rotational rates. The fiber diameters were 9.5 ± 4.8 μm (for 2000 rpm), 8.6 ± 2.8 μm (for 3000 rpm), and 5.2 ± 3.7 μm (for 4000 rpm). Varying the rotational rate from 2000 to 4000 rpm increased the centrifugal force such that the fiber diameter was reduced and the fiber diameter distribution became narrower. The thinnest fiber diameter of 5.2 ± 3.7 μm was obtained at 4000 rpm; however, the rotational rate at which jet break-up also occurred and beads were formed varied. A rate of 3000 rpm in association with a polymer concentration of $C/C^* = 5$ (15 wt%) gave fibers having a smooth morphology with no beads. In addition, a rate of 2000 rpm gave the same fiber morphology with a broadening of the fiber diameter distribution.

The fiber morphology can also be affected by the internal nozzle diameter. Three types of nozzles with internal diameters
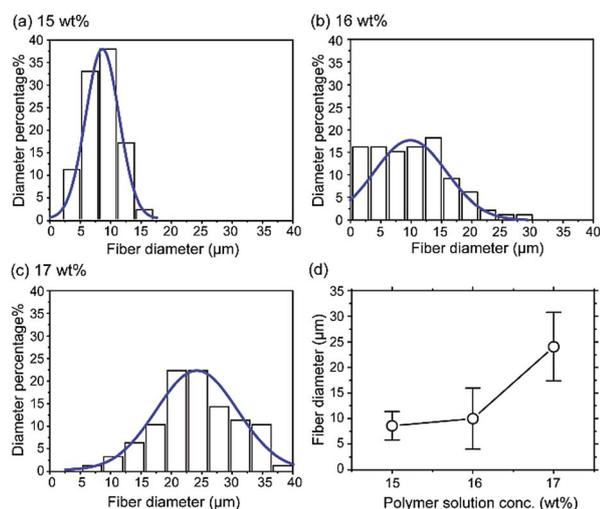

Fig. 4 Fiber diameter distributions of the 6-nitro BIPS/PMMA forcespinning fibers prepared with different polymer solution concentrations: (a) 15, (b) 16, and (c) 17 wt%. The final graph plots the average fiber diameter of the fibers as a function of the polymer solution concentration. Forcespinning conditions: 290 mm distance between needle and collectors, 0.34 mm 23 G needle nozzle, spinneret rotational rate of 3000 rpm.
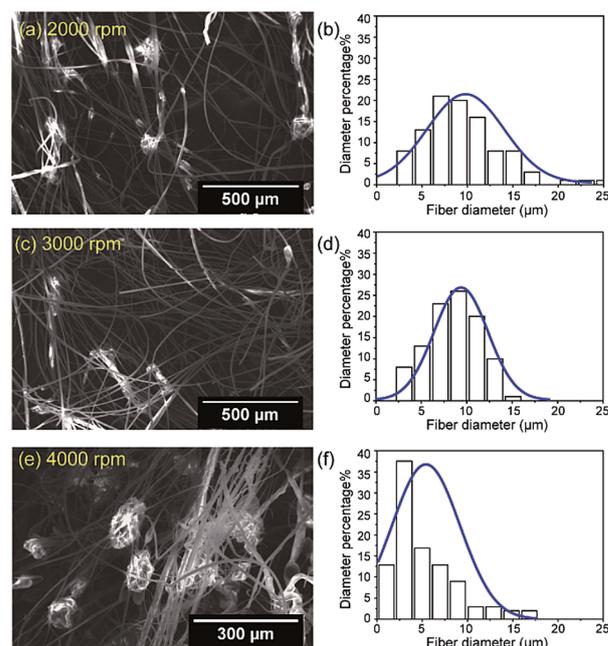

Fig. 5 SEM images and fiber diameter distributions of 6-nitro BIPS/PMMA forcespinning fibers prepared with spinneret rotational rates of: (a and b) 2000 rpm, (c and d) 3000 rpm, and (e and f) 4000 rpm. Forcespinning conditions: 290 mm distance between needle and collectors, 0.34 mm 23 G needle nozzle, 15 wt% polymer solution concentration.

of 0.34 (23 G), 0.26 (25 G), and 0.18 mm (28 G) were used to study the relationship between fiber morphology and nozzle diameter, using a 290 mm distance between the needle and collectors, a rotational rate of 3000 rpm and a 15 wt% polymer solution concentration. The SEM images of these specimens (not shown) indicate diameters of 8.6 ± 2.8 μm (for 23 G), 2.5 ± 1.4 μm (for 25 G), and 2.4 ± 1.2 μm (for 28 G). The data therefore indicate that a decrease in internal nozzle diameter leads to smaller mass throughput, which restricts the fiber diameter.

These results imply that the fiber morphology and diameter are influenced by several variables, including temperature, internal nozzle diameter, and needle/collectors distance. However, the main factors are the concentration of the polymer solution (hence the viscosity) and the rotational rate. These factors are in agreement with published reports.[19–22] The morphology of the fibers is evidently most strongly affected by the concentration of the polymer solution.

The forcespinning technique can be readily applied to the addition of a functional dye (typically a photochromic or fluorescence dye) to polymers, if such dyes are highly soluble in an organic solvent. This can produce, for example, functionalized fibers that undergo reversible color changes. In order to evaluate the kinetics of color changes based on photo-induced ring-opening, we employed color-strength, using the K/S peak value based on reflectance, indicating the actual color not affected by individual differences. For this purpose, 6-nitro BIPS/PMMA forcespinning fibers were fabricated using a 15 wt% solution, 3000 rpm, and a 23 G nozzle. The **SP**-form of the 6-nitro BIPS in the fibers exhibited essentially no K/S peak in the visible region prior to irradiation with 360 nm light. After continuous irradiation at 360 nm, the fibers turned purple and a new K/S peak appeared at 573 nm and increased in size as time progressed. This color change indicates that the spirocarbon–oxygen (C–O) bond of the **SP**-form was cleaved, and that subsequent photoisomerization gave the colored PMC-form, with a zwitterionic structure.[23] The K/S peak at 573 nm was monitored as a function of irradiation time, and the results are shown in Fig. 6(a). A photograph of the 6-nitro BIPS/PMMA forcespinning fibers after irradiation at 360 nm light is also presented in Fig. 6(b). Before light irradiation, the main K/S peak of the **SP**-form was present in the range of 320–400 nm (data not shown). This peak is assigned to π–π^* transitions of chromene and indoline rings. After irradiation, the K/S peak of the PMC-form gradually decreased over approximately 60 min at ambient temperature, as shown in Fig. 6(c). A photograph of the 6-nitro BIPS/PMMA forcespinning fibers after thermal decoloration in the dark is provided in Fig. 6(d). The purple-colored fibers in the photograph demonstrate the irradiated area, while the white fibers are the non-irradiated regions. The maximum absorbance of the PMC-form in films based on non-polar matrices appears at 600 nm, whereas the maximum absorbance in films based on polar matrices (such as PMMA) is with the absorption peak normally seen in PMMA films.[24] In polar matrices, the PMC-form is predominantly comprised of charge-localized zwitterionic structures that are stabilized in such matrices. Nadolski *et al.* have suggested that the singlet ground state is more polar than the singlet excited state,[25] therefore, the PMC-form is
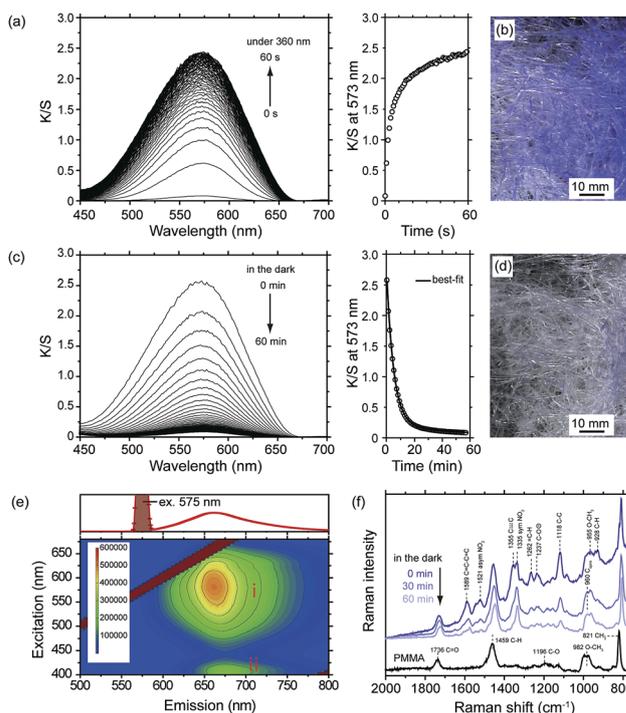

Fig. 6 Kubelka–Munk spectra of 6-nitro BIPS/PMMA forcespinning fibers obtained using the following forcespinning conditions: 15 wt% polymer solution concentration, spinneret rotational rate of 3000 rpm, 290 mm distance between needle and collectors, 0.34 mm 23 G needle nozzle. (a) Spectral changes and growth profile of the K/S peak at 573 nm during irradiation with 360 nm light (0–60 s, 1 s intervals). (b) Photograph showing aspect of the 6-nitro BIPS/PMMA forcespinning fibers after 360 nm light irradiation. (c) Spectral changes and decay profile of the K/S peak at 573 nm in the dark (0–60 min, 1 min intervals). (d) Photograph showing aspect of the 6-nitro BIPS/PMMA forcespinning fibers under dark condition at 60 min after 360 nm light irradiation. (e) Fluorescence EEM (emission wavelength 500 to 800 nm, step size 5 nm; excitation wavelength 400 to 680 nm, step size 1 nm) of the PMC-form in the PMMA forcespinning fibers. (f) Raman (785 nm) spectra of 6-nitro BIPS/PMMA forcespinning fibers after thermal decoloration in the dark.

stabilized against external heating in polar matrices, which results in a short-wavelength shift (that is, a hypsochromic shift).[26,27]

Typical plots showing K/S growth and relaxation (decoloration) processes are presented in Fig. 6(a) and (c). The kinetic characteristics of this process can be described by a biexponential function:

$$K/S_t = K/S_0 + a(1 - e^{-k_1 t}) + b(1 - e^{-k_2 t}).$$

In this equation, K/S_t is the change in K/S at 573 nm observed at time t, K/S_0 is the residual K/S at 573 nm at infinity, and a and b are the fractions of the PMC-form with decoloration rate constants k_1 and k_2. These rate constants respectively indicate the fast and slow decoloration processes. The rate constants and the fractions were obtained by fitting the experimental curve in Fig. 6(c) (right). The PMC-form in the PMMA

forcespinning fibers faded with rate constants of $k_1 = 3.2 \times 10^{-3}$ s^{-1} and $k_2 = 5.8 \times 10^{-4}$ s^{-1}. In addition, the amplitude fractions of the fast and slow decoloration components were 0.92 and 0.08, respectively. These rate constants are associated with the relaxation of isolated and aggregated PMC-forms, respectively.[28,29] These results indicate that isolated 6-nitro BIPS is primarily incorporated in the interiors of the fibers and predominantly contributes to the total decoloration process. In contrast, the aggregated 6-nitro BIPS is distributed near the fiber surfaces, which stabilizes the PMC-form. PMC aggregation is often observed in conjunction with decoloration processes. As an example, the PMC-form immobilized on the surface of silica spheres was found to fade with rate constants of $k_1 = 4.2 \times 10^{-3}$ s^{-1} and $k_2 = 1.3 \times 10^{-3}$ s^{-1}, attributed to the isolated and aggregated forms, respectively.[30] The fluorescence EEM spectrum of the PMC-form in the PMMA forcespinning fibers is shown in Fig. 6(e). The EEM spectra can be divided into 2 regions as follows: region I with intense emission (ex/em: 530–630 nm/641–687 nm) corresponding to the PMC-form, and region II with weak emission (ex/em: 400–425 nm/662–690 nm) corresponding to PMC-form being in intermolecular energy transfer from the indoline ring. When the PMC-form in the PMMA forcespinning fibers is excited with 575 nm light, strong pale red emission centered at 662 nm is obtained as shown in the upper part of the Fig. 2(e). When the PMC-form in the PMMA forcespinning fibers is excited with 400–425 nm light, emission is shaped similar to that with 530–630 nm excitation, and almost no peak shift is obtained. The fluorescence quantum yield Φ_F for the PMC-form in the PMMA forcespinning fibers is determined to be $\Phi_F = 0.15$, which is slightly higher than that in PMMA films ($\Phi_F = 0.10$).[31] The results of fluorescence EEM spectrum and fluorescence quantum yield indicate that the PMC-form is stabilized in the fiber environment and restricted conformational flexibility, which would minimize nonradiative relaxation through internal motions of the excited PMC-form in the PMMA forcespinning fibers.

Fig. 6(f) shows the Raman spectra of the decoloration process of the PMC-form in the PMMA forcespinning fibers corresponding to the K/S decoloration (Fig. 6(c)). The Raman spectrum of the PMMA forcespinning fibers not containing the 6-nitro BIPS shows the many similar peaks in the Raman shift region (from 657 cm^{-1} to 2736 cm^{-1}) with a PMMA in bulk.[32] According to the literature, Raman peak associated with C=O stretching appears at 1736 cm^{-1}; C–H bending at 1459 cm^{-1}; C–O stretching at 1196 cm^{-1}; O–CH$_3$ stretching at 982 cm^{-1}; CH$_3$ rocking at 821 cm^{-1} and C–O bending at 677 cm^{-1}. The Raman spectrum of the 6-nitro BIPS/PMMA forcespinning fibers just after 360 nm light irradiation is denoted as 0 min. The Raman spectra for the PMC-form in the PMMA forcespinning fibers were measured in the dark at room temperature. The Raman spectrum at 0 min shows several new Raman peaks at 1589, 1521, 1355, 1335, 1262, 1237, 1118, and 960 cm^{-1} in addition to the Raman peaks of PMMA forcespinning fibers. These peaks are ascribed to C=C–C=C indoline stretching (1589 cm^{-1}); asymmetric NO$_2$ stretching (1521 cm^{-1}); C–C partial double bond (1355 cm^{-1}); symmetric NO$_2$ stretching (1335 cm^{-1}); =C–H bending (1262 cm^{-1}); C–O$^-$ stretching

(1237 cm^{-1}); C–C stretching (1118 cm^{-1}) and C–H (928 cm^{-1}) of the PMC-form. After stopping the 360 nm light irradiation, the Raman peaks at 1118, 1237 and 1262 cm^{-1} associated with the PMC-form gradually decreased while the Raman peak of O–C$_{spiro}$–N (960 cm^{-1}) associated with the SP-form increases.

The decoloration mechanism in these fibers is in good agreement with observations on silica surfaces that have been reported previously. The most notable finding herein regarding the forcespinning technique is that it is possible to make fibers and nonwoven fabrics using the same techniques as are applied when making films, because the majority of the PMC-form is present in the isolated state. Consequently, because forcespinning fibers can be mass-produced at low cost, this technique should have numerous applications, in particular for smart textiles.

Conclusions

In conclusion, a forcespinning apparatus of our own design was fabricated, based on the Forcespinning® system marketed by the FibeRio Technology Co., with the aim of producing low-cost micro/nano fibers on a large scale. The fiber morphology was found to be greatly affected by the concentration/viscosity of the polymer solution, just as is the case with electrospinning or standard forcespinning systems. The resulting SP-functionalized PMMA forcespinning fibers were capable of undergoing reversible color changes in response to irradiation at 360 nm. The photochromic properties of these fibers were similar to those found in polymeric film. Thus, the physical and chemical properties of dye-doped forcespinning fibers can be evaluated in the same manner as those of films. The forcespinning technique should widen the range of applications of color changing textiles technologies and may assist in improving the design of smart textiles as well as producing technical and functional clothing.

Acknowledgements

References

1 R. Nayak, R. Padhye, I. L. Kyratzis, Y. B. Truong and L. Arnold, *Text. Res. J.*, 2011, **82**(2), 129–147.

2 Q. P. Pham, U. Sharma and A. G. Mikos, *Tissue Eng.*, 2006, **12**(5), 1197–1211.

3 R. Gopal, S. Kaur, Z. Ma, C. Chan, S. Ramakrishna and T. Matsuura, *J. Membr. Sci.*, 2006, **281**(1), 581–586.

4 S. Kedem, J. Schmidt, Y. Paz and Y. Cohen, *Langmuir*, 2005, **21**(12), 5600–5604.

5 X. Wang, C. Drew, S.-H. Lee, K. J. Senecal, J. Kumar and L. A. Samuelson, *Nano Lett.*, 2002, **2**(11), 1273–1275.

6 X. Wang, H. Niu and T. Lin, *Polym. Eng. Sci.*, 2009, **49**, 1582–1586.

7 S. Padron, A. Fuentes, D. Caruntu and K. Lozano, *J. Appl. Phys.*, 2013, **113**(2), 024318.

8 K. Sarkar, C. Gomez, S. Zambrano, M. Ramirez, E. de Hoyos, H. Vasquez and K. Lozano, *Mater. Today*, 2010, **13**(10), 12–14.

9 B. Weng, F. Xu and K. Lozano, *J. Appl. Polym. Sci.*, 2015, **132**, 42535.

10 Z. Ming-Qiang, Z. Linyong, J. H. Jason, W. Wuwei, K. H. James and D. Q. L. Alexander, *J. Am. Chem. Soc.*, 2006, **128**(13), 4303–4309.

11 C. Alvarez-Lorenzo, L. Bromberg and A. Concheiro, *Photochem. Photobiol.*, 2009, **85**(4), 848–860.

12 J. R. Hemmer, P. D. Smith, M. van Horn, S. Alnemrat, B. P. Mason, J. R. de Alaniz, S. Osswald and J. P. Hooper, *J. Polym. Sci., Part B: Polym. Phys.*, 2014, **52**, 1347–1356.

13 H. Tsuchida, R. Nakamura, K. Kinashi, W. Sakai, N. Tsutsumi, M. Ozaki and T. Okabe, *New J. Chem.*, 2016, **40**, 8658–8663.

14 K. Kinashi, Y. Miyamae, R. Nakamura, W. Sakai, N. Tsutsumi, H. Yamane, G. Hatsukano, M. Ozaki, K. Jimbo and T. Okabe, *Chem. Commun.*, 2015, **51**, 11170–11173.

15 R. Klajn, *Chem. Soc. Rev.*, 2014, **43**, 148–184.

16 B. L. Hager and G. C. Berry, *J. Polym. Sci., Polym. Phys. Ed.*, 1982, **20**(5), 911–928.

17 C. Tanford, *Physical Chemistry of Macromolecules*, Wiley, New York, 1961.

18 P. Gupta, C. Elkins, T. E. Long and G. L. Wilkes, *Polymer*, 2005, **46**, 4799–4810.

19 Z. McEachin and K. Lozano, *J. Appl. Polym. Sci.*, 2012, **126**(2), 473–479.

20 S. Padron, A. Fuentes, D. Caruntu and K. Lozano, *J. Appl. Phys.*, 2013, **113**(2), 024318.

21 B. Weng, F. Xu, A. Salinas and K. Lozano, *Carbon*, 2014, **75**, 217–226.

22 N. Obregon, V. Agubra, M. Pokhrel, H. Campos, D. Flores, D. De la Garza, Y. Mao, J. Macossay and M. Alcoutlabi, *Fibers*, 2016, **4**(2), 20.

23 K. Kinashi, T. Horiguchi, K. Tsutsui, K. Ishida and Y. Ueda, *J. Photochem. Photobiol., A*, 2010, **213**, 189–193.

24 J.-S. Lin and H.-T. Chiu, *J. Polym. Res.*, 2003, **10**, 105–110.

25 B. Nadolski, P. Uznanski and M. Kryszewski, *Makromol. Chem., Rapid Commun.*, 1984, **5**, 327–331.

26 K. Kinashi, S. Nakamura, Y. Ono, K. Ishida and Y. Ueda, *J. Photochem. Photobiol., A*, 2010, **213**, 136–140.

27 M. Miura, T. Hayashi, F. Akutu and K. Nagakubo, *Polymer*, 1978, **19**, 348–349.

28 H. R. Allcock and C. Kim, *Macromolecules*, 1991, **24**, 2846–2851.

29 E. Goldburt, F. Shvartsman and V. Krongauz, *Macromolecules*, 1984, **17**, 1876–1878.

30 M. Ueda, K. Kudo and K. Ichimura, *J. Mater. Chem.*, 1995, **5**, 1007–1011.

31 K. Kinashi, Y. Ono, Y. Naitoh, A. Otomo and Y. Ueda, *J. Photochem. Photobiol., A*, 2011, **217**, 35–39.

32 I. Blaszczyk-Lezak, M. Hernández and C. Mijangos, *Macromolecules*, 2013, **46**, 4995–5002.